Journal of the Endocrine Society, 2023, **7**, 1–7
https://doi.org/10.1210/jendso/bvad022
Advance access publication 6 February 2023
Research Article

Altered Expression of Several Molecular Mediators of Cerebrospinal Fluid Production in *Hyp* Mice

Jared Kaplan,[1] Steven Tommasini,[2] Gang-Qing Yao,[1] Meiling Zhu,[1] Sayoko Nishimura,[3] Sevanne Ghazarian,[1] Angeliki Louvi,[3,*] and Karl Insogna[1,*]

[1]Department of Internal Medicine, Yale School of Medicine, New Haven, CT 06520-8020, USA
[2]Department of Orthopaedic Surgery, Yale School of Medicine, New Haven, CT 06520-8020, USA
[3]Departments of Neurosurgery and Neuroscience, Yale School of Medicine, New Haven, CT 06520-8020, USA

Correspondence: Karl Insogna, MD, Department of Internal Medicine, Yale School of Medicine, 300 Cedar St, S-141, P.O. Box 208020, New Haven, CT 06520-8020, USA. Email: karl.insogna@yale.edu.
*These authors contributed equally to this work.

Abstract

Context: X-linked hypophosphatemia (XLH) is a genetic disease, causing life-long hypophosphatemia due to overproduction of fibroblast growth factor 23 (FGF23). XLH is associated with Chiari malformations, cranial synostosis, and syringomyelia. FGF23 signals through FGFR1c and requires a coreceptor, α-Klotho, which is expressed in the renal distal convoluted tubules and the choroid plexus (ChP). In the ChP, α-Klotho participates in regulating cerebrospinal fluid (CSF) production by shuttling the sodium/potassium adenosine triphosphatase (Na^+/K^+-ATPase) to the luminal membrane. The sodium/potassium/chloride cotransporter 1 (NKCC1) also makes a substantial contribution to CSF production.

Objective: Since CSF production has not been studied in XLH, we sought to determine if there are changes in the expression of these molecules in the ChP of *Hyp* mice, the murine model of XLH, as a first step toward testing the hypothesis that altered CSF production contributes to the cranial and spinal malformations seen this disease.

Methods: Semi-quantitative real-time PCR was used to analyze the level of expression of transcripts for Fgfr1c, and thee key regulators of CSF production, Klotho, Atp1a1 and Slc12a2. In situ hybridization was used to provide anatomical localization for the encoded proteins.

Results: Real-time polymerase chain reaction (RT-PCR) demonstrated significant upregulation of *Klotho* transcripts in the fourth ventricle of *Hyp* mice compared to controls. Transcript levels for *Fgfr1c* were unchanged in *Hyp* mice. *Atp1a1* transcripts encoding the alpha-1 subunit of Na^+/K^+-ATPase were significantly downregulated in the third and lateral ventricles (LV). Expression levels of the *Slc12a2* transcript (which encodes NKCC1) were unchanged in *Hyp* mice compared to controls. In situ hybridization (ISH) confirmed the presence of all 4 transcripts in the LV ChP both of WT and *Hyp* mice.

Conclusion: This is the first study to document a significant change in the level of expression of the molecular machinery required for CSF production in Hyp mice. Whether similar changes occur in patients with XLH, potentially contributing to the cranial and spinal cord abnormalities frequently seen in XLH, remains to be determined.

Key Words: X-linked hypophosphatemia (XLH), choroid plexus, CSF, Klotho, FGF23

Abbreviations: cDNA, complementary DNA; ChP, choroid plexus; CSF, cerebrospinal fluid; FGF23, fibroblast growth factor 23; ISH, in situ hybridization; LV, lateral ventricle; Na^+/K^+-ATPase, sodium/potassium ATPase; NKCC1, sodium/potassium/chloride cotransporter 1; PFA, paraformaldehyde; PHEX, phosphate-regulating endopeptidase homologue X-linked; RT, room temperature; RT-PCR, real-time polymerase chain reaction; WT, wild-type; XLH, X-linked hypophosphatemia.

X-linked hypophosphatemia (XLH; OMIM No. 307800) is a hereditary form of renal phosphate wasting caused by loss-of-function mutations in the phosphate-regulating endopeptidase homolog X-linked (*PHEX*) gene, resulting in elevated levels of fibroblast growth factor 23 (FGF23). FGF23 binds to the alpha-klotho (α-Klotho)-FGF receptor R1c complex in the renal tubular cell to suppress renal phosphate reabsorption. This results in lifelong hypophosphatemia, causing skeletal and dental disease. Chiari malformations and cranial synostosis have been reported to occur with high frequency in XLH [1–3], in addition to anterior and posterior longitudinal ligament calcification and syringomyelia [4, 5].

Although FGF23 is predominantly secreted by osteoblasts and osteocytes in bone, it is also expressed by other cell types in tissues, such as brain and teeth [6, 7]. α-Klotho is a type-1 transmembrane protein that is expressed in the distal convoluted tubule of the kidney, the parathyroid gland, and the choroid plexus (ChP) [8]. In the ChP, α-Klotho plays a central role in regulating cerebrospinal fluid (CSF) production [9]. In the kidney, parathyroid gland, and ChP, α-Klotho has been shown to participate in the cellular trafficking of the sodium/potassium adenosine triphosphatase (Na^+/K^+-ATPase) pump [9]. Notably, α-Klotho participates in a complex with the Na^+/K^+-ATPase subunits alpha-1 (to which it binds) and beta to facilitate shuttling of the pump to the plasma membrane [9]. It has also been suggested

Received: 5 October 2022. **Editorial Decision:** 27 January 2023. **Corrected and Typeset:** 17 February 2023

that a fraction of cellular Na^+/K^+-ATPase is trafficked from the endoplasmic reticulum to the cell surface, chaperoned by α-Klotho in recycling endosomes.

Although the exact mechanisms of CSF production have yet to be fully elucidated, it is thought that a wide range of transporters expressed in the ChP participate. In the ChP epithelium, Na^+/K^+-ATPase and sodium/potassium/chloride cotransporter 1 (NKCC1) function in a coordinated fashion by establishing an osmotic gradient and facilitating active water transport, respectively [10]. Consistent with its important role in CSF production, inhibiting the Na^+/K^+-ATPase with ouabain reduces CSF production by 50% [11]. The exact mechanism by which NKCC1 participates in CSF production is complex and appears to be influenced by the concentration of potassium in the CSF [10, 12, 13, 14].

The *Hyp* mouse bears a loss-of-function mutation in *Phex* and has elevated serum levels of FGF23 [15]. It exhibits all the key biochemical, histologic, and skeletal manifestations of XLH, including craniofacial abnormalities [16–18]. α-Klotho expression is reduced in the kidneys of *Hyp* mice [19]. We wondered whether similar changes occurred in the ChP of these animals and whether other components of the CSF production machinery were also altered by genetic absence of *Phex*.

Materials and Methods

Materials

Paraformaldehyde, sucrose, phosphate buffer, EDTA, and proteinase K were from Sigma-Aldrich. Superfrost/Plus slides were from Thermo Fisher Scientific. Slide mailers were from Baxter Scientific. Primers and probes for real-time polymerase chain reaction (RT-PCR) used to quantitate expression levels of *Klotho*, *Fgfr1c*, *Atp1a1*, *and Slc12a2* were from Applied Biosystems. Supplementary Table S1 lists the ABS assays used [20]. The probes for in situ hybridization were prepared using the Ambion MEGAscript kit, and digoxigenin-11-UTP from Boehringer Mannheim, following the manufacturer's instructions.

Probes for In Situ Hybridization

Murine complementary DNAs (cDNAs) were amplified by reverse transcription -PCR using a kit from Bio-Rad. PCR primer sequences and expected product sizes for the probes amplified from *Fgfr1c*, *Klotho*, *Atp1a1*, *and Slc12a2*, are listed in Table 1. PCR products were cloned into the pCR II-TOPO vector (Invitrogen). The cloned plasmid DNAs were linearized with appropriate restriction enzymes, purified, and transcribed to synthesize sense or antisense complementary RNA probes using T7 or SP6 RNA polymerase.

Animals

Hyp (*Phex*^{Hyp}, Mouse Genome Informatics) mice and wild-type (WT) littermates were maintained in C57BL/6J background as a breeding colony. All studies were approved by the Institutional Animal Care and Use Committee at Yale University.

Methods

In situ hybridization

Adult *Hyp* and WT littermate control mice were deeply anesthetized with ketamine-xylazine. Brains were then fixed by intracardiac perfusion with 4% paraformaldehyde (PFA, Sigma Aldrich, P6148), extracted, cryoprotected by immersion in 30% sucrose in 4% PFA, and sectioned (36 μm) using a cryomicrotome (Leica Microsystems). Sections were mounted on Superfrost/Plus slides in 0.5× phosphate buffer (Sigma-Aldrich), dried overnight at room temperature (RT) and processed immediately. All subsequent treatments, including hybridization, were carried out in slide mailers. Sections were fixed again in freshly prepared 4% PFA for 20 minutes at RT, followed by 3 washes in DEPC-PBS at RT. Sections were then incubated for 30 minutes in detergent solution (1% IGEPAL CA-630, 1% SDS, 0.5% deoxycholate, 50.0 mM Tris-HCl pH 8.0, 1.0 mM EDTA pH 8.0, 150 mM NaCl) twice at RT, followed by a 10-minute wash in DEPC-PBS. Sections were then treated with 1 μg/mL proteinase K in buffer containing 100 mM Tris-HCL, pH 8.0, and 50 mM EDTA for 30 minutes at 37 °C. This was followed by fixation in 4% PFA for 15 minutes at RT, followed by a DEPC-PBS rinse. Sections were hybridized with digoxigenin-11-UTP-labeled-antisense RNA probes for mouse *Klotho*, *Fgfr1c*, *Atp1a1*, and *Slc12a2*. To confirm specificity, digoxigenin-11-UTP-labeled-sense RNA probes were also hybridized for *Klotho* and *Fgfr1c*. Sections were analyzed using a Stemi 2000-C stereomicroscope or AxioImager (Zeiss) fitted with an AxioCam MRc5 digital camera. Images were captured using AxioVision software (Zeiss) and assembled in Adobe Photoshop. Data using sense probe controls are provided in Supplementary Fig. S1 [20].

Isolation of choroid plexus

Mice were anesthetized with ketamine-xylazine and euthanized by cervical dislocation in accordance with institutional animal care and use committee guidelines. ChP tissue was excised from individual ventricles (lateral [LV], third, and fourth) and placed into 2-mL Safelock Eppendorf tubes containing 1 mL TRIzol and one 5-mm stainless steel bead. Excised samples were then immediately snap-frozen in liquid nitrogen and stored at −80 °C until RNA isolation. For this study, 15 *Hyp* animals (7 females, 8 males) and 10 littermate controls (7 females, 3 males) were used to isolate ChP tissue.

RNA isolation and real-time polymerase chain reaction

Excised ChP tissue was homogenized for 30 seconds using a Qiagen TissueLyser II (Qiagen) in the 2-mL Safelock Eppendorf tubes just described to which had been added a 5-mm stainless steel bead (Qiagen). RNA was then extracted using TRIzol (Invitrogen) according to the manufacturer's protocol and purified with a Qiagen RNeasy minikit. Reverse transcriptase-polymerase chain reaction was used to generate cDNAs according to standard techniques. RT-PCR was performed using these cDNAs amplified with Taq polymerase (Roche Diagnostic Corp) and the TaqMan assays listed in Supplementary Table S1 [20].

Statistical Analyses

All statistical analyses were performed using GraphPad Prism v7.0 software. Unpaired 2-tailed *t* test was used to calculate significance. Data are presented as mean ± SEM. The error bars in figures reflect SEM. A value of at least *P* less than .05 was considered to indicate a statistically significant difference.

Table 1. Primers and probes for in situ hybridization

Gene symbol	Protein	Primer	Probe size, bp
Fgfr1c	Fibroblast growth factor receptor 1	GGAGGTACGGAGCCTTGTTA TGTCTGGCCCGATCTTACTC	954
Kl	α-Klotho	CCCACTACCGCTTCTCCATA CTGTAGCCCCTATGCCACTC	979
Atp1a1	Alpha1 subunit of ATPase Na^+/K^+	TTGGAGAACGTGTGCTAGGT CCGATCTGTCCATAGGCCAT	931
Slc12a2	Na-K-Cl cotransporter, also called solute carrier 12a2	TATTGGAGCCATTACAGTCGTG TGGTCTGAAGTTTTTCACATGG	1135

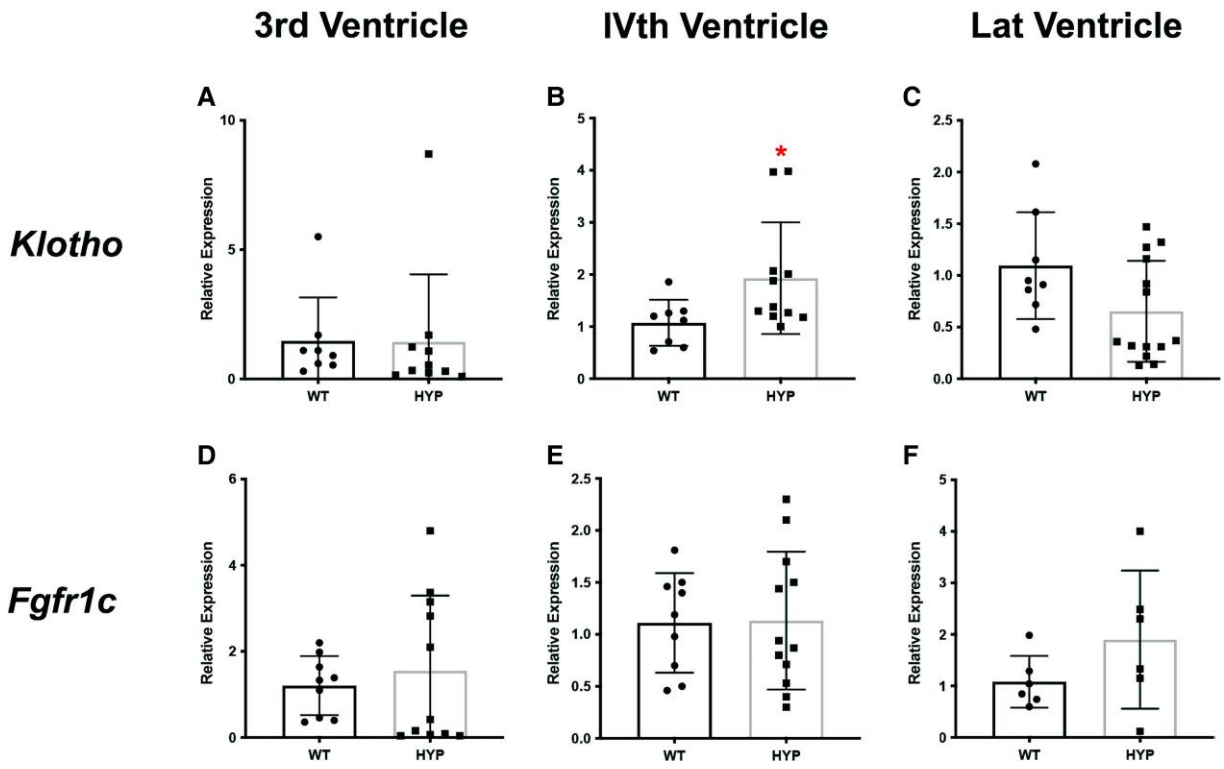

Figure 1. The mean level of expression in wild-type (WT) animals was used as a reference to estimate levels of *Klotho* and *Fgfr1c* in individual samples taken from the same ventricle of *Hyp* mice third (3rd), fourth (IVth), and lateral (LV) ventricles. A, n = 8 WT, 10 *Hyp*; B, n = 8 WT, 11 *Hyp*; C, n = 8 WT, 14 *Hyp*; D, n = 9 WT, 11 *Hyp*; E, n = 9 WT, 12 *Hyp*; F, n = 6 WT, 6 *Hyp*. Numbers indicate the number of choroid plexus isolates analyzed. Data are expressed as M ± SEM; **P* less than .05, calculated using an unpaired 2-tailed *t* test.

Results

Changes in Expression Profiles of *Atp1a1*, *Slc12a2*, *Klotho*, and *Fgfr1c* in the Choroid Plexus of *Hyp* Mice

RT-PCR demonstrated a statistically significant increase in expression of *Klotho* in the fourth ventricle of *Hyp* mice compared to controls (Fig. 1B). Expression of *Klotho* was not significantly different between controls and *Hyp* mice in the third and LV (Fig. 1A and 1C). In the LV the apparent reduction in *Kloto* expression in the *Hyp* mice compared to controls just missed statistical significance (Fig. 1C; $P = .059$). Expression of *Fgfr1c* was not significantly different between *Hyp* mice and controls (Fig. 1D-1F). Expression of *Atp1a1* in ChP was significantly suppressed in the third and LV of Hyp mice compared to controls (Fig. 2A and 2C). Expression levels of *Slc12a2* were unchanged in all 3 ventricles of *Hyp* mice compared to control animals (Fig. 2D-2F).

Expression of *Atp1a1*, *Slc12a2*, *Klotho*, and *Fgfr1c* by In Situ Hybridization

To provide anatomical correlates to the changes observed in expression for *Atp1a1*, *Slc12a2*, *Klotho*, and *Fgfr1c*, we performed ISH for the respective transcripts in the LV of *Hyp* mice and WT controls. As observed in Fig. 3A, there was intense *Klotho* staining, with a regular, cobblestone appearance throughout the ChP in the LV of WT animals. Although *Klotho* was also expressed in the LV of *Hyp* mice (Fig. 3B), the cobbled appearance was less evident. *Fgfr1c* was expressed throughout the ChP in the LV of both *Hyp* controls (Fig. 3C and 3D). Staining for this receptor was also observed in the hippocampal formation (pyramidal layer; Fig. 3C and 3D, white arrows). *Atp1a1* expression was observed throughout the ChP of the LV of *Hyp* mice and controls (Fig. 4A and 4B). Expression of

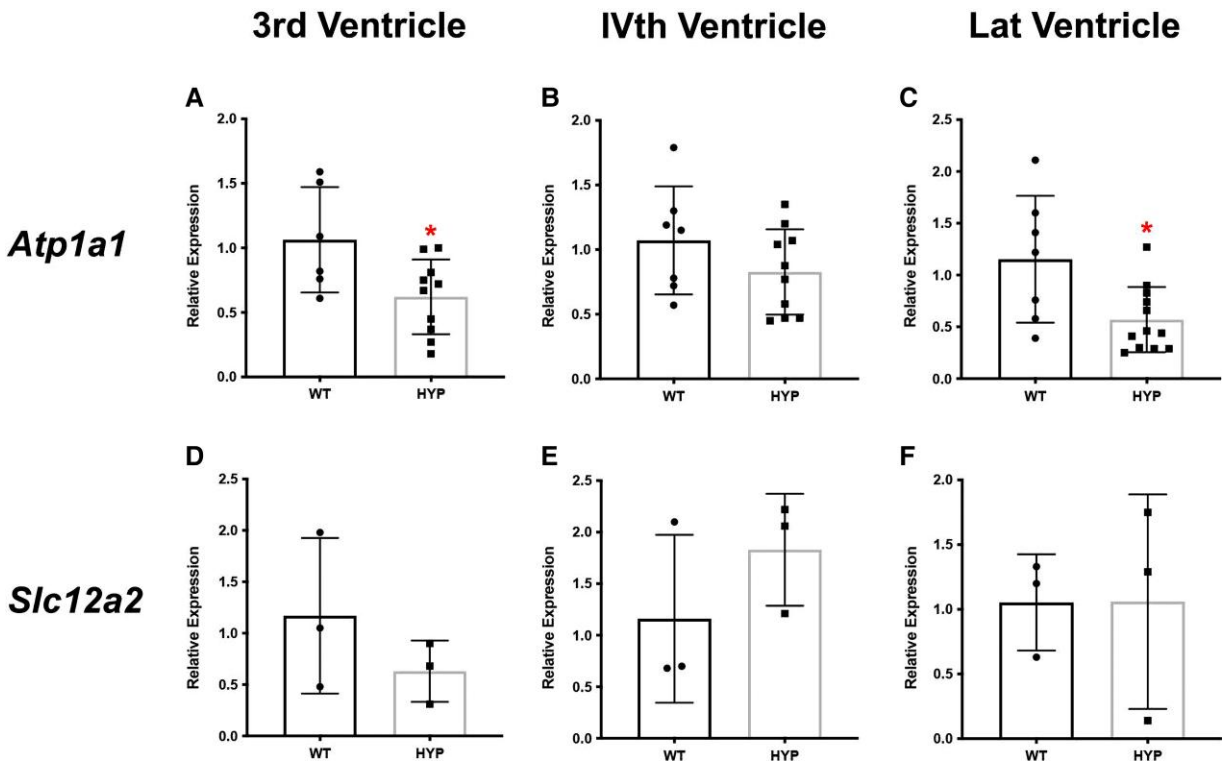

Figure 2. The mean level of expression in wild-type (WT) animals was used as a reference to estimate levels of *Atp1a1* and *Slc12a2* in individual samples taken from the same ventricle of *Hyp* mice: third ventricle (3rd), fourth ventricle (IVth), and lateral ventricles (LV). A, n = 6 WT, 10 *Hyp*; B, n = 7 WT, 10 *Hyp*; C, n = 7 WT, 12 *Hyp*; D through F, n = 3 WT, 3 *Hyp*. Numbers indicate the number of choroid plexus isolates analyzed. Data are expressed as M ± SEM; **P* less than .05, calculated using an unpaired 2-tailed *t* test.

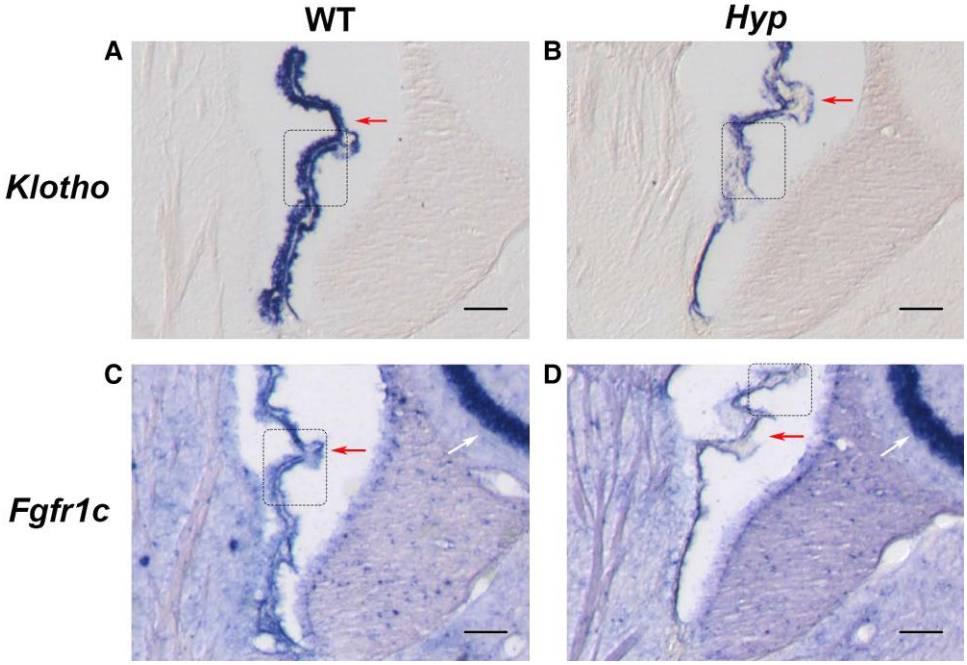

Figure 3. In situ hybridization for *Klotho* in the lateral ventricle ChP (red arrows) of A, wild-type (WT) and B, *Hyp* mice and for *Fgfr1c* (red arrows) in C, WT and D, *Hyp* mice. The pyramidal layer, identified by the white arrow, also expresses FGFR1c. Scale bar represents 200 μM. Higher magnifications of the boxed areas are shown in Supplementary Fig. S3 [20].

this cotransporter was also observed in the hippocampal formation (Fig. 4A, white arrow). Staining for *Slc12a2* (NKCC1) was observed in the LV of *Hyp* mice as well as controls (Fig. 4C and 4D). Although changes in staining intensity for the 4 transcripts were observed by ISH, this technology is not amenable to

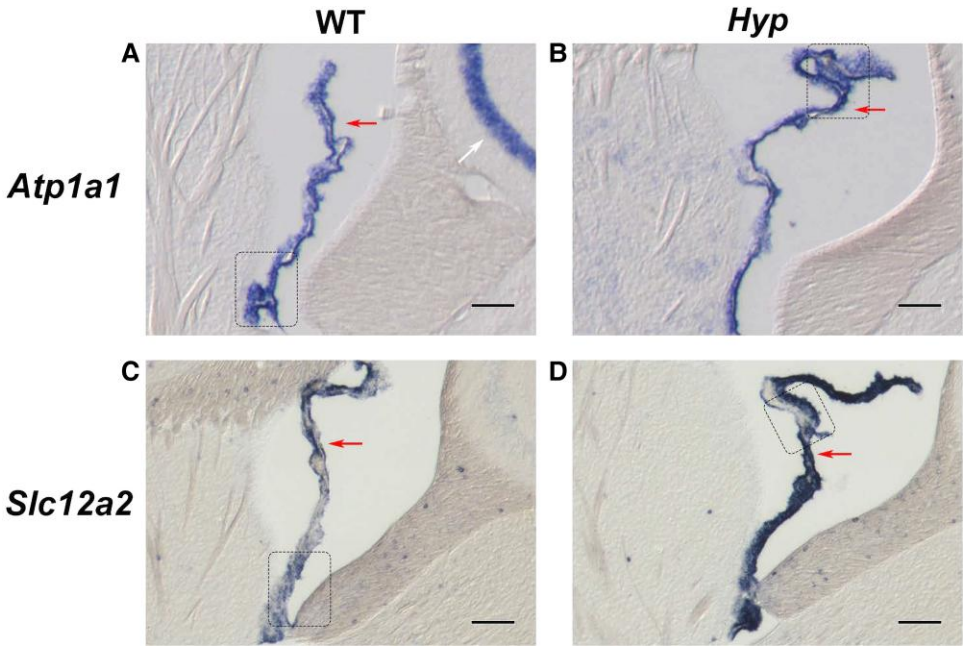

Figure 4. In situ hybridization for *Atp1a1* in the lateral ventricle (red arrows) of A, wild-type (WT) and B, *Hyp* mice and for *ATP1a1* (red arrows) in C, WT and D, *Hyp* mice and for *Slc12a2* in C, WT and D, *Hyp*. The pyramidal layer also stains for *ATP1a1* (white arrow). Scale bar represents 200 μM. Higher magnifications of the boxed areas are shown in Supplementary Fig. S4 [20].

precise quantification. The RT-PCR data provide a better estimate of the actual expression of these molecules in the ChP.

Discussion

This study is the first to demonstrate changes in the expression of key components of the cellular machinery that direct the production of CSF in *Hyp* mice. We observed a significant reduction in the expression of *Atp1a1* in the third and LV of Hyp mice compared to controls. This transcript encodes the alpha subunit of Na^+/K^+-ATPase, one of the key molecular participants in CSF production. In the kidney, active transport of sodium phosphate into the cell from the lumen via sodium phosphate–dependent cotransporters is driven by the downhill sodium gradient maintained by the Na^+/K^+-ATPase at the basolateral surface of the cell, which pumps sodium out of the cell.

The ChP is often referred to as the "kidney of the brain" because much of the same machinery is conserved, albeit with membrane orientation inverted. In the kidney, the Na^+/K^+-ATPase is on the basolateral surface and the electrochemical gradient flows from apical to basolateral. In the ChP, however, the Na^+/K-ATPase is on the apical surface and the electrochemical gradient flows from basolateral to apical. Available evidence suggests that α-Klotho is responsible for trafficking Na^+/K^+-ATPase to the cell membrane [9]. By RT-PCR, α-Klotho was marginally reduced in the LV ($P = .059$) and expression of *Atp1a1* was significantly suppressed in the LV of Hyp mice compared to controls. As noted earlier, expression of α-Klotho is reduced in the *Hyp* kidney. On a mass basis the LV ChP is presumably a major site of CSF production. Taken together, these data suggest that ATP1a1-driven CSF production might be reduced in the *Hyp* mouse.

NKCC1 has also been reported to play an important role in CSF production. In particular, Steffensen et al [10] found that after administration of bumetanide, a potent inhibitor of NKCC1, CSF production was reduced by approximately half. Inhibiting the Na^+/K^+-ATPase with ouabain also reduces CSF production by approximately 50% [11]. Na^+/K^+-ATPase and NKCC1 are thought to function in a coordinated fashion to drive production of CSF. NKCC1 functions independently of the overall osmotic gradient by coupling water transport to the movement of sodium, potassium, or chloride ions down their respective electrochemical gradients. In contrast to the findings of Steffensen et al, Gregoriades and colleagues [12] reported that NKCC1 mediates CSF clearance. To explain these divergent findings, Gregoriades et al [12] used driving force calculations to show that the different concentrations of intracellular sodium used in these 2 studies explain the differences in the reported mode of action of NKCC1. Delpire and Gagnon [13] have suggested that NKCC1-mediated transport fluctuates between inward and outward directions depending on physiological conditions. A recent study by Xu et al [14] supports this dynamic model. These authors reported increased CSF clearance during early mouse postnatal development due to the combined effect of a high CSF potassium concentration and overexpression of NKCC1.

By RT-PCR there was no change in the expression of *Slc12a2*, which encodes the NKCC1 cotransporter, in the *Hyp* mice. In view of the findings of Steffensen et al [10] and Gregoriades et al [12], one could postulate that CSF production in *Hyp* mice is further impaired by the actions of NKCC1. One possibility is that reduced ATP1a1-dependent CSF production, coupled with unaltered, or perhaps enhanced, NKCC1-mediated clearance, would markedly impair CSF production. Whether similar changes occur in patients with XLH is unknown, but leaves open the possibility that aberrant CSF production is intrinsic to the disease process.

Shetty and Meyer [18] reported significant craniofacial abnormalities in *Hyp* mice, with shorter skulls that had a domed appearance. Prominent bulges were seen in frontonasal and

premaxillary-maxillary sutures. We are not aware of data directly demonstrating a pathogenic role for altered CSF production in the development of the cranial abnormalities that are seen both in patients with XLH and in *Hyp* mice. Nonetheless, a speculative but intriguing hypothesis is that reduced CSF production in the genetic absence of *Phex* plays a direct pathogenic role in the skeletal and spinal cord pathology not infrequently observed in XLH [1–5].

We found expression of *Fgfr1c* in the ChP. It has been previously reported that this receptor is expressed in the central nervous system [21–25] but it had not been previously identified in ChP. Membrane-bound α-Klotho has been shown to localize to the apical membrane in the ChP [26, 27]. Our RT-PCR data demonstrated that the expression level of α-Klotho transcript was increased in the fourth ventricle and marginally decreased in the LV of *Hyp* mice. These data indicate that both components of the signaling complex required for the action of FGF23 are present in the ChP. Whether canonical FGF23 signaling occurs in this tissue, and whether signaling is altered in *Hyp* mice by elevated circulating levels of FGF23 as well as changes in α-Klotho expression, are intriguing possibilities.

In summary, this is the first study to document changes in the level of expression of some of the molecular machinery required for CSF production in *Hyp* mice. How or if these changes contribute to the cranial and spinal cord malformations that frequently afflict patients with XLH warrants further study.

Funding

This work was supported by the Yale Bone Center (to K.L.I.) and in part by the National Institutes of Health (grant R21 NS052718 to A.L.).

Disclosures

S.T. serves as a scientific advisor for Acantha Medical. K.I. receives support from Ultragenyx for industry-sponsored and investigator-initiated research. ST and KI both attest that that their identified support does not conflict in any way with the current study. All other authors state that they have no conflicts of interest.

Data Availability

Original data generated and analyzed during this study are included in this published article or in the data repositories listed in "References."

References

1. Rothenbuhler A, Fadel N, Debza Y, *et al.* High incidence of cranial synostosis and Chiari I malformation in children with X-linked hypophosphatemic rickets (XLHR). *J Bone Miner Res*. 2019;34(3):490-496.
2. Caldemeyer KS, Boaz JC, Wappner RS, Moran CC, Smith RR, Quets JP. Chiari I malformation: association with hypophosphatemic rickets and MR imaging appearance. *Radiology*. 1995;195(3):733-738.
3. Vega RA, Opalak C, Harshbarger RJ, *et al.* Hypophosphatemic rickets and craniosynostosis: a multicenter case series. *J Neurosurg Pediatr*. 2016;17(6):694-700.
4. Chesher D, Oddy M, Darbar U, *et al.* Outcome of adult patients with X-linked hypophosphatemia caused by *PHEX* gene mutations. *J Inherit Metab Dis*. 2018;41(5):865-876.
5. Watts L, Wordsworth P. Chiari malformation, syringomyelia and bulbar palsy in X linked hypophosphataemia. *BMJ Case Rep*. 2015;2015:bcr2015211961. Doi:10.1136/bcr-2015-211961
6. Yamashita T, Yoshioka M, Itoh N. Identification of a novel fibroblast growth factor, FGF-23, preferentially expressed in the ventrolateral thalamic nucleus of the brain. *Biochem Biophys Res Commun*. 2000;277(2):494-498.
7. Yoshiko Y, Wang H, Minamizaki T, *et al.* Mineralized tissue cells are a principal source of FGF23. *Bone*. 2007;40(6):1565-1573.
8. Kuro-o M, Matsumura Y, Aizawa H, *et al.* Mutation of the mouse klotho gene leads to a syndrome resembling ageing. *Nature*. 1997;390(6655):45-51.
9. Imura A, Tsuji Y, Murata M, *et al.* α-Klotho as a regulator of calcium homeostasis. *Science*. 2007;316(5831):1615-1618.
10. Steffensen AB, Oernbo EK, Stoica A, *et al.* Cotransporter-mediated water transport underlying cerebrospinal fluid formation. *Nat Commun*. 2018;9(1):2167.
11. Holloway L Jr, Cassin S. Effect of acetazolamide and ouabain on CSF production rate in the newborn dog. *Am J Physiol*. 1972;223(3):503-506.
12. Gregoriades JMC, Madaris A, Alvarez FJ, Alvarez-Leefmans FJ. Genetic and pharmacological inactivation of apical Na^+-K^+-$2Cl^-$ cotransporter 1 in choroid plexus epithelial cells reveals the physiological function of the cotransporter. *Am J Physiol Cell Physiol*. 2019;316(4):C525-C544.
13. Delpire E, Gagnon KB. Elusive role of the Na-K-2Cl cotransporter in the choroid plexus. *Am J Physiol Cell Physiol*. 2019;316(4):C522-C524.
14. Xu H, Fame RM, Sadegh C, *et al.* Choroid plexus NKCC1 mediates cerebrospinal fluid clearance during mouse early postnatal development. *Nat Commun*. 2021;12(1):447.
15. Strom T, Francis F, Lorenz B, *et al. Pex* gene deletions in *Gy* and *Hyp* mice provide mouse models for X-linked hypophosphatemia. *Hum Mol Genet*. 1997;6(2):165-171.
16. Liang G, VanHouten J, Macica CM. An atypical degenerative osteoarthropathy in *Hyp* mice is characterized by a loss in the mineralized zone of articular cartilage. *Calcif Tissue Int*. 2011;89(2):151-162.
17. Zhang H, Chavez M, Kolli T, *et al.* Dentoalveolar defects in the *Hyp* mouse model of X-linked hypophosphatemia. *J Dent Res*. 2020;99(4):419-428.
18. Shetty NS, Meyer RA Jr. Craniofacial abnormalities in mice with X-linked hypophosphatemic genes (*Hyp* or *Gy*). *Teratology*. 1991;44(4):463-472.
19. Meyer MH, Dulde E, Meyer RA Jr. The genomic response of the mouse kidney to low-phosphate diet is altered in X-linked hypophosphatemia. *Physiol Genomics*. 2004;18(1):4-11.
20. Kaplan J, Tommasini S, Yao GQ, *et al.* Supplemental materials for "Altered expression of several molecular mediators of cerebral spinal fluid production in *Hyp* mice." Data can be accessed at https://doi.org/10.5281/zenodo.7558718. Date of upload 23 January 2023.
21. Matsuo A, Tooyama I, Isobe S, *et al.* Immunohistochemical localization in the rat brain of an epitope corresponding to the fibroblast growth factor receptor-1. *Neuroscience*. 1994;60(1):49-66.
22. Belluardo N, Wu G, Mudo G, Hansson A, Pettersson R, Fuxe K. Comparative localization of fibroblast growth factor receptor-1, -2, and -3 mRNAs in the rat brain: in situ hybridization analysis. *J Comp Neurol*. 1997;379(2):226-246.
23. Gaughran F, Payne J, Sedgwick PM, Cotter D, Berry M. Hippocampal FGF-2 and FGFR1 mRNA expression in major depression, schizophrenia and bipolar disorder. *Brain Res Bull*. 2006;70(3):221-227.
24. Reid S, Ferretti P. Differential expression of fibroblast growth factor receptors in the developing murine choroid plexus. *Dev Brain Res*. 2003;141(1-2):15-24.

25. Szmydynger-Chodobska J, Chun ZG, Johanson CE, Chodobski A. Distribution of fibroblast growth factor receptors and their co-localization with vasopressin in the choroid plexus epithelium. *Neuroreport*. 2002;13(2):257-259.
26. Li SA, Watanabe M, Yamada H, Nagai A, Kinuta M, Takei K. Immunohistochemical localization of Klotho protein in brain, kidney, and reproductive organs of mice. *Cell Struct Funct*. 2004;29(4):91-99.
27. Pavlatou M, Remaley A, Gold P. Klotho: a humeral mediator in CSF and plasma that influences longevity and susceptibility to multiple complex disorders, including depression. *Transl Psychiatry*. 2016;6(8):e876.